A Light Puncture Robot for CT and MRI Interventions

Designing a New Robotic Architecture to Perform Abdominal and Thoracic Punctures

BY IVAN BRICAULT, NABIL ZEMITI, EMILIE JOUNIAUX, CÉLINE FOUARD, ÉLISE TAILLANT, FREDERIC DORANDEU, AND PHILIPPE CINQUIN

In the field of interventional radiology, image-guided percutaneous interventions are common procedures that are used for diagnostic or therapeutic purposes. Biopsies, abscess drainages, or tumor ablations can be performed percutaneously. The clinical demand for such interventions is growing as they are minimally invasive and as they are often able to prevent the need for a surgical intervention.

The first step in interventional radiology is the puncture of a target, which can be an anatomical structure or a tumor, and whose diameter is generally 1 cm or greater, a dimension considered to be clinically significant. These percutaneous punctures can be complicated procedures. The needle insertion is most often controlled with computer tomography (CT), but the planned trajectory can be particularly difficult to implement and to track by the radiologist on CT images when the needle is not aligned with a simple direction of the image plane. Indeed, tilted insertion paths are sometimes advised to avoid organs or ribs. Several attempts may be necessary to reach the target, causing a loss of time and more traumas than expected to the patient. Moreover, both the radiologist and the patient are exposed to X-rays when CT is used to guide the puncture process in real time.

Compared with CT, magnetic resonance imaging (MRI) is a promising nonirradiating imaging modality for the real-time control of a puncture, but specific constraints apply in an MRI environment, particularly, because of the magnetic field and the limited access to the patient allowed by traditional closed MRI devices. The diameter of the bore does not exceed 60 cm, a space that is also occupied by the patient.

The use of robots for surgical interventions is an approach that has been proven to increase the quality of operations and to establish new types of surgical procedures [1]. In the context of interventional radiology, puncture robots may be very helpful. They have the potential to work within CT or MRI and to decrease the intervention duration while providing optimal accuracy and safety to patients.

These factors have motivated our research in the development of a new lightweight robot, for abdominal and thoracic percutaneous procedures, which is compatible with CT, open MRI, and closed MRI. Our aim is to control, in real time, the initial positioning of the needle and the puncture movement itself. Thus, the robot has to be able to operate alone, but with remote medical supervision, inside the CT or magnetic resonance (MR) guidance imaging device.

This robot (Figure 1), named Light Puncture Robot (LPR), has an original compact body-supported architecture, which is naturally able to follow the patient's body surface respiratory movements. It is entirely made of plastic and uses MR-compatible pneumatic actuators powered by compressed air. It is localized via an image-based control using a localization device that is totally integrated to the robot. The physician is also included in the control loop, since he/she selects the target and the entry point and supervises the whole process.

Related Work

Since the early 1990s, more than 35 surgical robotic systems have been developed [1]. In the field of MRI interventional robotics, there exists, to our knowledge, only one commercial MR-compatible system: the Innomotion robot for percutaneous interventions [23]. It is a six degrees of freedom (DoF) fully MR-compatible pneumatic robot that has been optimized for use in closed-bore MRI and CT scanners [2]. However, the current version of the system provides only position guidance, i.e., the robot indicates to the physician the insertion point and the needle orientation. For closed-bore MRI interventions, it is difficult to advance the needle manually inside the magnet bore. The patient table has to be moved outside the bore to perform the puncture correctly.

However, if the robot is mounted to the table and not body supported by the patient (which is the case of the Innomotion system), any nonintentional movement of the patient during the table displacement may make changes in the planned needle trajectory with respect to the desired one. Consequently, as we cannot have real time needle guidance outside the MR bore, such robot architecture is not robust with respect to patient movement and might cause injury to the patient.

Other MRI interventional robots are currently available at research laboratories. The major challenge for the development of these systems is the MR compatibility [3]–[5]. For further details about MR compatibility questions, see [24].

Digital Object Identifier 10.1109/EMB.2007.910262

The robot has to be able to operate alone inside the CT or MRI device.

Several research groups have developed MR-compatible robots actuated by ultrasonic motors. Although these actuators are not affected by the magnetic field, their encasings contain conductive material that result in substantial image artefacts if placed just near the MR magnet [6]. Shielding or placing these motors inside a Faraday cage does not eliminate the artefacts [7]. Such actuators could be placed far away from the MR magnet as in [8] and [9], where MR-compatible robots were used for biopsy and therapeutic interventions in the breast, and in [10], where a novel MR-compatible manipulator design for prostate intervention was detailed. One can note that, for such specific clinical applications, it is possible to have long distance interaction between the control unit (ultrasonic motors) outside the MRI magnet and the patient inside the magnet. However, in the general case, this configuration is not suitable since it decreases the rigidity of the system, as has been emphasized in [11].

Electrostatic motors could also be used within an MR environment. Compared with ultrasonic motors, they should interfere less with MRI [12]. However, as the electrostatic motor is driven by a three-phase ac high-voltage source, it still requires developments on the power electronics to be used in the operation room.

Alternatively, a hydrostatic transmission approach is proposed in [6]. The concept is based on a telemanipulator system with a mechanical transmission between the master (conventional actuator outside the magnet shield) and the slave made from MR-compatible polymers. Another robot, named the MrBot [2], was recently developed at the Johns Hopkins University, which uses a new type of pneumatic step motor (the PneuStep) specifically designed for MRI application. This robot is highly specialized. It is customized for transperineal needle insertion for the prostate gland under either open- or closed-bore MRI scanners.

In [13], it is shown that the devices constructed using binary polymer-based actuators, called electrostrictive polymer actuators, are able to function within the MRI without degrading its imaging performance. The binary nature of these actuators eliminates the need for feedback sensors for motion control. Their construction is fundamentally inexpensive and simple. They can be constructed essentially from plastic, making their potential cost low enough to be disposable. This attractive approach remains to be explored further.

The LPR Architectural Design: Answers to CT/MRI Compatibility and Safety Issues

The LPR architecture is mainly based on the previous works done at the Techniques de l'Ingénierie Médicale et de la Complexité (TIMC) Laboratory on the Tele-Echography Robot [14] and the Light Endoscopy Robot [15]. It is lightweight (1 kg), compact (15×23 cm^2), and its installation is particularly simple, so that the necessary setup time is greatly reduced.

As shown in Figure 1, the main feature of this robot is its original body-supported architecture [16], which suppresses the risk of accidental trauma on the patient's body by robot or needle parts. Indeed, since the robot follows the patient's abdomen/thorax surface, this concept provides an intrinsic compensation for some physiological or unexpected movements of the patient. Moreover, during the puncture step itself, i.e., when the needle is moved toward its internal target, an apnea identical to the one performed during the last image acquisition is required from the patient. If not, external body movements due to respiration may not be correlated with internal organ breathing movements and may interfere with the planned needle trajectory.

This concept of placing the robot on the patient has been chosen also in [17] and [18] for endoscopic surgery (the MC^{2}E robot), in [19] for percutaneous cholecystostomy interventions (the UMI system), and in [20] for CT-guided percutaneous interventions (the CT-Bot system).

The LPR possesses five DoF and is composed of two parts. The main part, the needle-holder that is laid directly on the

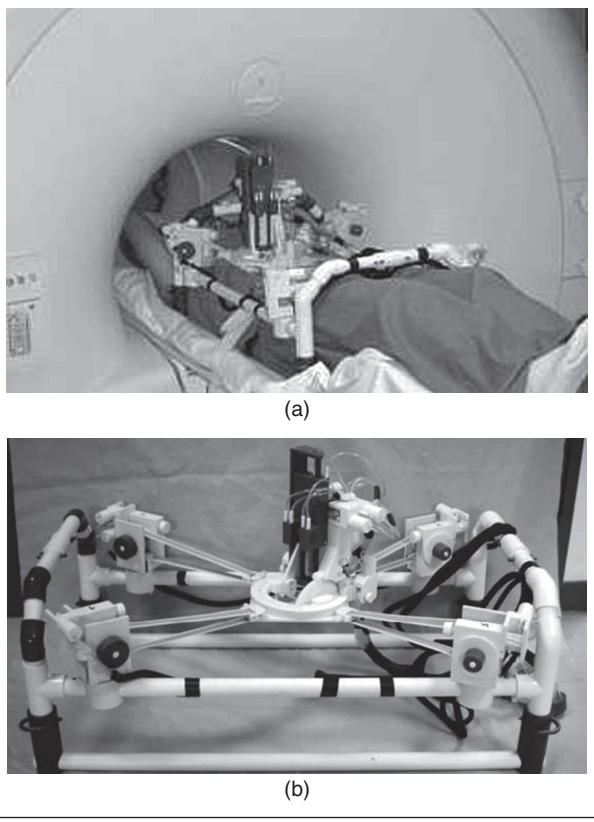

Fig. 1. The LPR. (a) The LPR on a patient during an MRI examination. (b) The entire LPR robot.

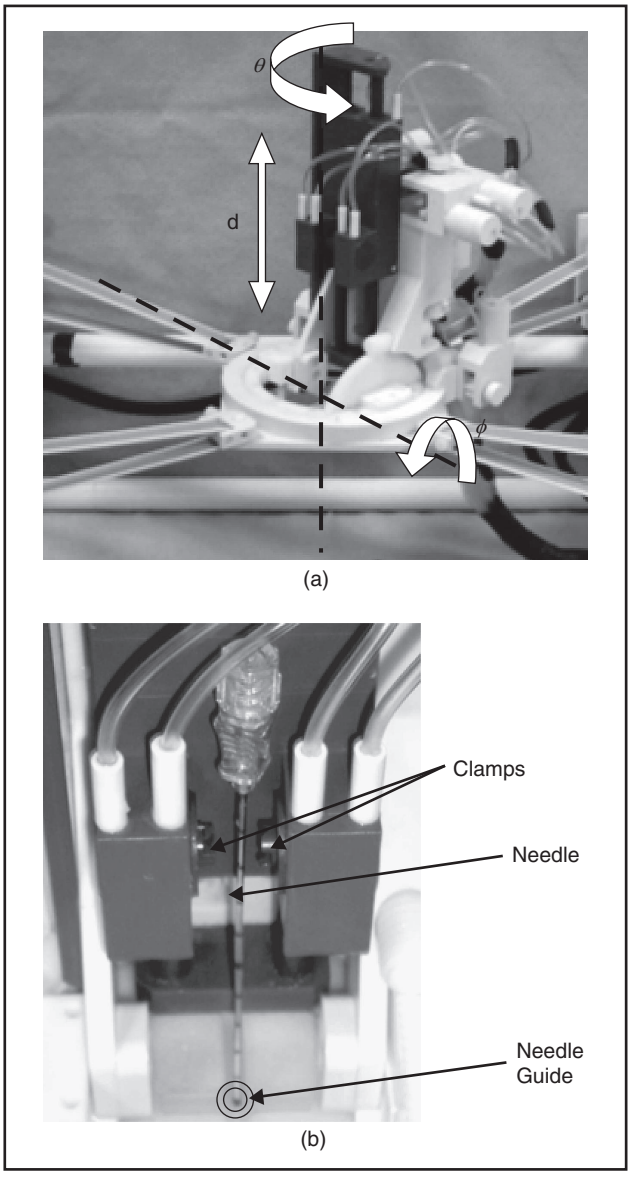

Fig. 2. The LPR needle holder. (a) DoF of the needle holder. (b) The needle-holder puncture part.

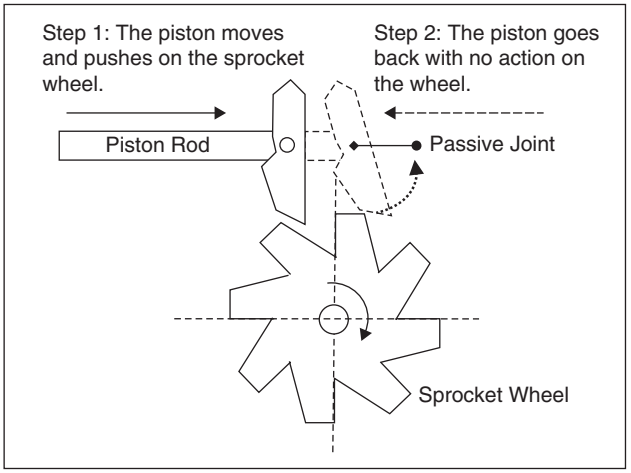

Fig. 3. The principle of the pneumatic actuator for controlling the LPR movement.

patient's body, provides three DoF [Figure 2(a)]: a translation $d \in [0, 9\text{ cm}]$ along the needle axis, a rotation $\theta \in [0, 2\pi]$ with respect to the robot's platform and around an axis normal to the patient's body, and an inclination $\phi \in [-\pi/18, \pi/3]$ of the needle holder with respect to the robot's base.

The second part of the robot is composed of a support frame and four actuators that provide the two remaining DoF, i.e., the translation over the patient's body, which gives natural standoff and orientation to the robot [Figure 1(b)]. This movement is done with the help of four straps. Each strap is bounded to the needle-holder platform on one side and to the actuators on the other side. The architecture of the support frame of LPR offers the possibility of making a height adjustment of 10 cm to adapt the robot to the patient's corpulence and to the imaging system size.

The LPR is made of plastic materials (nylon, delrin, and epoxy) that have been chosen to ensure MR compatibility and a minimum of artefacts under the CT environment [3], [7]. The LPR's MR compatibility has been checked on a clinical MR equipment (Achieva 1.5 T, Philips Medical Systems), initially, without any patient and, then, while imaging the robot placed over the abdomen of a volunteer [Figure 1(a)]. Various clinical MR sequences, routinely used for abdominal imaging, have been tested: standard (fast-field echo) and three-dimensional (3-D) volume interpolated [T1W high-resolution isotropic volume examination (THRIVE)] breath-hold gradient-echo T1-weighted acquisitions as well as breath-hold and respiratory-triggered turbo spin-echo T2-weighted acquisitions. In each case and as expected, LPR plastic components generated no signal in the images and caused no artefacts on the adjacent abdominal organs. As part of future work, this qualitative evaluation will be complemented by additional quantitative tests including signal-to-noise ratio (SNR) measurements.

Contrary to other anthropomorphic robots with a plastic long arm, in the case of a modular and very compact system such as the LPR robot, the rigidity of the overall system is guaranteed. To be totally compatible with the MR environment, compressed air is used as an energy source. The robot controller and air compressor are linked to the actuators by 7-m-long plastic tubes, allowing them to be placed outside the MR room, beyond the magnetic hazard zone.

A new and original way of using pneumatic actuators, based on clock-making principles, was developed. Each actuator is composed of two sets of pistons and cylinders, one for each movement direction. On each side of the cylinder, one air inlet brings the compressed air (four-bar pressure) to the piston. Air is alternatively injected in each compartment. The first step consists in moving the piston and pushing the associated sprocket wheel by one increment. The second step consists in making the piston return back without any action on the wheel through the use of a passive joint (Figure 3). This incremental movement is rated at a maximum frequency of three impulses per second. This movement is possible only in one direction, thus permitting the user to block the robot in a certain position. A worm gear is assembled to the sprocket wheel axis and works with its corresponding gear (Figure 4). For translation, the actuators have a pulley that allows the straps to be entangled or disentangled (Figure 5). The actuators can also be disengaged to perform a manual prepositioning of the needle holder when the robot is installed on the patient.

The needle-holder puncture part [Figure 2(b)] includes clamps used to grasp the needle and a translation unit (a fast

The main feature of this robot is its original body-supported architecture.

linear pneumatic actuator), which is able to perform a fast puncture in a single motion (above 9 cm/s) to perforate the skin or organs walls. To guarantee that the puncture movement will be straight, the needle is inserted through a guide (a small, drilled ball) placed at the center of the robot base.

The puncture depth (i.e., the distance from the entry point to the targeted point) is controlled via a thrust bearing that stops the motion of the fast linear actuator. The locations of the entry point and the target point have to be specified by the physician during the path planning, thus defining the desired position of the thrust bearing. This position can be precisely controlled with a resolution of 0.16 mm using a slow pneumatic actuator based on clock-making principles running at three impulses per second (piston + sprocket wheel).

If the target distance from the entry point is greater than the needle-holder stroke (9 cm), the robot can perform a deeper insertion by releasing the needle and grasping it higher. When it is released by the clamps, the needle can follow the movements of the patient's target organ, thus avoiding injuries. This approach also offers the possibility of performing the needle insertion in several steps, which is identical to the way the physician would work manually. Between each new motion step, the physician has the opportunity to check and, eventually, update the desired needle trajectory.

Ideally, the robot might automatically grasp the needle again after it has been released. To do so, we can ask the patient to reproduce identical apneas before each needle regrasping, which is supposed to replace the needle at the same position where it was released just before, i.e., at the center of the clamping mechanism. However, in practice, one cannot guarantee the success of this operation. In fact, nonreproducible apnea can occur, which results in the needle moving away from the clamping mechanism. Consequently, physician supervision is mandatory when performing deeper insertions by releasing the needle and grasping it higher.

Although the insertion velocity and force cannot be controlled with the current needle holder, this system is clinically adequate for percutaneous interventions, since it is possible to precisely control the needle penetration depth and to produce a sufficient insertion force to safely penetrate the patient's skin and tissues. The force and velocity capabilities of the LPR insertion device (80 N for the force and 9 cm/s for the velocity) are satisfactory with regard to the stiffness of the patient skin and tissues and also the duration of the patient apnea, which should not exceed 10 s for optimal patient comfort.

Finally, this method allows a very easily and precisely controlled movement of the different parts of the robot. The overall robot specifications are summarized in Table 1.

Robot Position Control

An important issue for robot guidance is the precise localization of the end effector in the intraoperative space. To do so,

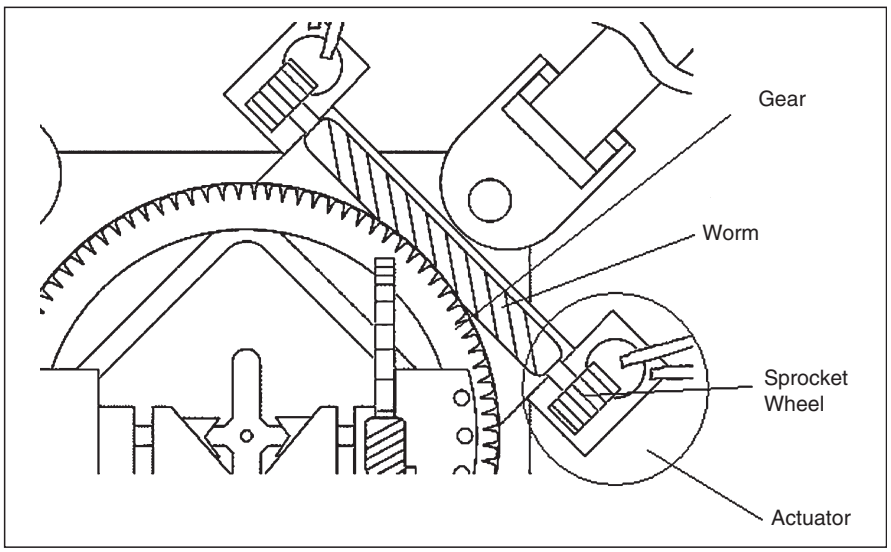

Fig. 4. Needle-holder rotation actuator.

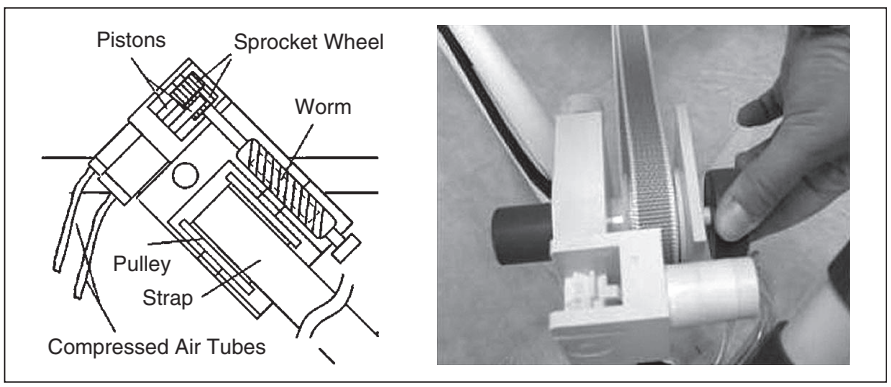

Fig. 5. The principle of the translating actuator.

and as an alternative to conventional position encoders, localization modules are usually placed on the robot or its end effector [20], [21]. Here, we also designed a specific localization device that can be used to compute the LPR planar position and orientation (the three translational and rotational DoF) according to the CT/MR reference. This localization device is a square frame made of epoxy resin ensuring CT visibility and is filled with oil for MR visibility (Figure 6). It is rigidly fastened with screws to the proximal end of the rotating base of the robot so that it is totally integrated into the needle holder architecture. In the current robot design, this localization device does not follow the inclination movement of the needle holder, i.e., this fiducial does not give information about the needle inclination. To do so, the alternative adopted solution is to place the robot, at the beginning of each experiment, in an initial configuration corresponding to a 90° inclination of the needle with respect to the localization device in the robot base. Then, the control system relies on this a priori knowledge of the initial position to keep track of the current needle inclination after each inclination movement command.

Each time we want to know the robot position to check if it is correct, we have to acquire a set of images. Then, the images are automatically processed to detect the localization device and find the current orientation of the robot and the entry point. These images also allow the radiologist to confirm the adequate progression of the procedure.

LPR localization involves image-processing algorithms that have been developed and previously validated on CT images. CT acquisitions were performed on a four-slice Siemens CT scanner, reconstructing 2-mm-wide slices over a volume of 4 cm or more to acquire images over at least two-thirds of the localization device. The first step is a thresholding that leads to a binary image. A mathematical morphology closing operation comes next to fill in the holes in the image. Then, all the regions of the image are labeled in connected components, and a priori knowledge of the localization device geometry is applied to conserve only the points of interest. The size of all the connected objects is measured, and only objects whose area is smaller than the area of the longest diagonal of the localization device are kept. Furthermore, since the localization device is made of bars, its slices in the CT images are rectangular-shaped. We then use the ratio between the singular values of all object inertia ellipses to detect and keep only rectangle-shaped objects. These two treatments lead to images containing a large majority of localization device points for a minority of points of other objects [Figure 7(a) and (b)].

A Chamfer 3-D matching algorithm [22] is then used to register the segmented cloud of points with a 3-D model of the localization device [Figure 7(c)]. As a result, the registration parameters (rotation and translation) give the position and orientation of the localization device, i.e., the position of the robot and of the needle, since the geometric relationships between all these elements are precisely known.

Experimental Results

Initial experiments were performed on a plane surface inside a CT scan. They consisted in moving the robot to a particular position/inclination and measuring its positioning accuracy with a CT acquisition control. These experiments were performed 15 times. For each experience, the robot was moved between different initial and final positions or inclinations. For the robot base rotation and the needle-holder inclination tests, the expected angles were obtained with an angular error less than 1°.

Concerning the translation tests, we have obtained a strap-based translation accuracy of 5% of the displacement d; for instance, with $d = 20$ mm the maximum error was 1 mm.

Additionally, to evaluate the repeatability of the translation, each move was achieved back and forth four times; the same translation was achieved almost identically with a maximum variability of 0.5 mm.

Experiments on a phantom have shown the capacity of LPR to extract its exact position, using the localization device and image-processing algorithms, and to reach its target with millimeter accuracy. These experiments consisted in trying to reach a target from an unknown position and orientation of the robot, with a CT images' control. We used a 60 × 34 × 27 cm foam rubber block in which we inserted a polyether-cetone disc with a 1-cm hole as a target. Six punctures (two vertical and four with an arbitrary orientation) starting from different initial positions were performed; the depth for puncture varied from 4 to 6 cm. For each experiment, the robot was initially positioned

Table 1. Robot specifications.

Description	Value
Air pressure	4 bar
Needle driver maximum force capability	80 N
Needle penetration velocity (fast motion to reach the thrust bearing position)	9 cm/s
Actuators max. frequency (impulses per second)	3 Hz
Translational resolution (patient body plan)	0.1414 mm/impulse
Needle penetration resolution (incremental positioning of the thrust bearing)	0.15625 mm/impulse
Base rotation resolution	0.3°/impulse
Needle orientation resolution	0.375°/impulse
Base rotation range	$\theta \in [0, 2\pi]$
Needle orientation range	$\phi \in \left[\frac{-\pi}{18}, \frac{\pi}{3}\right]$

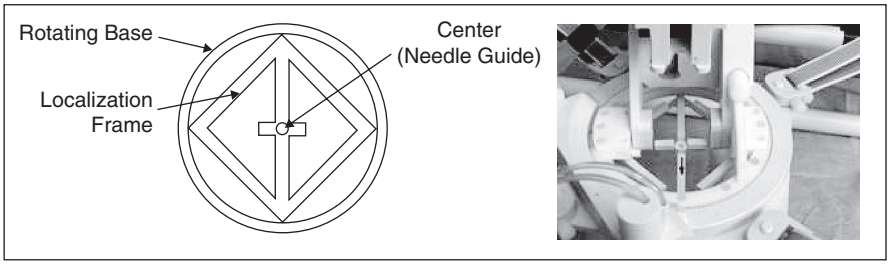

Fig. 6. The localization device.

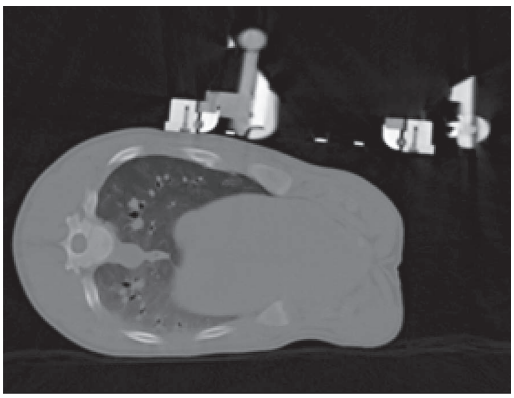

(a)

(b)

(c)

Fig. 7. Localization device segmentation and registration. (a) CT image acquired during animal experiments. (b) The thresholding step extracts parts from the localization device or from the rest of the robot and ribs. Geometric criteria succeed in selecting only parts from the localization device (in gray). (c) Schematic representation of the final matching step that registers the cloud of points extracted on CT images (dark to white points in this 3-D view of CT data) with a 3-D model of the localization device.

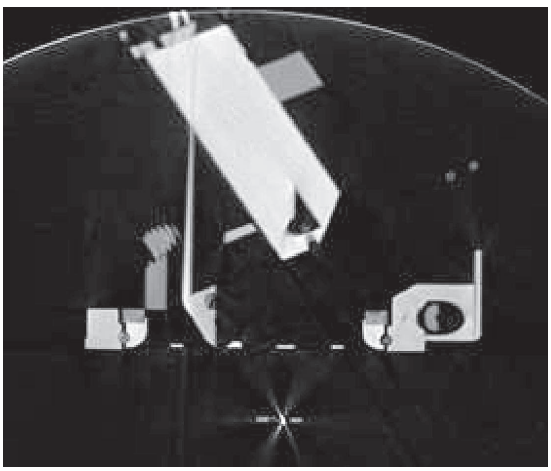

(a)

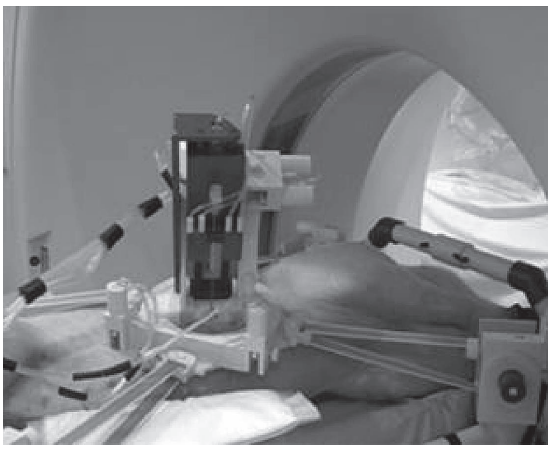

(b)

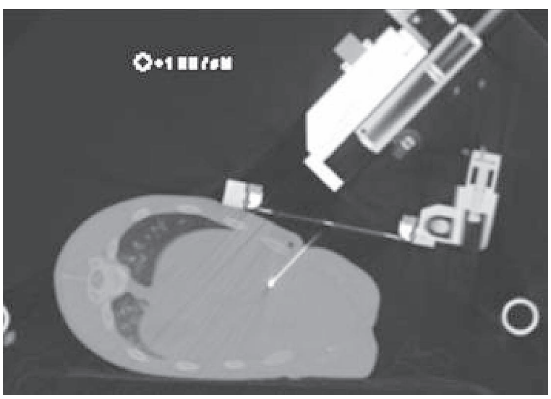

(c)

Fig. 8. Experimental results. (a) Puncture on phantom: the needle tip has successfully reached the center of the target, following an oblique out-of-plane path. (b) Setting for animal experiments. (c) Successful in vivo puncture of an artificially created target in a pig liver.

manually on the phantom in the rough vicinity of the desired puncture entry point. After a CT image acquisition, the LPR located itself and moved automatically to the user-defined position and orientation for puncture. This step was then checked by the operator on a second CT acquisition. In one case where the expected initial translation was large (5 cm),

the first robot movement did not exactly reach the expected entry point (translation error = 2 mm). Although such an inaccuracy would probably not be clinically significant, a second positioning command was given to the robot; the LPR then reached its expected position. In the other five cases (translation on a phantom surface between 1.5 and 3.5 cm), the robot position was judged to be satisfactory after the first step, and the puncture command could be given to the robot without further fine repositioning. In the final CT images acquired after the puncture, we then measured the distance between the tip of the needle and the target point (i.e., the center of the polyether-cetone disc). In all six cases, this distance was smaller than 2 mm (error range = 0.3–1.8 mm) so that the clinically significant 1-cm central hole target was correctly punctured [Figure 8(a)].

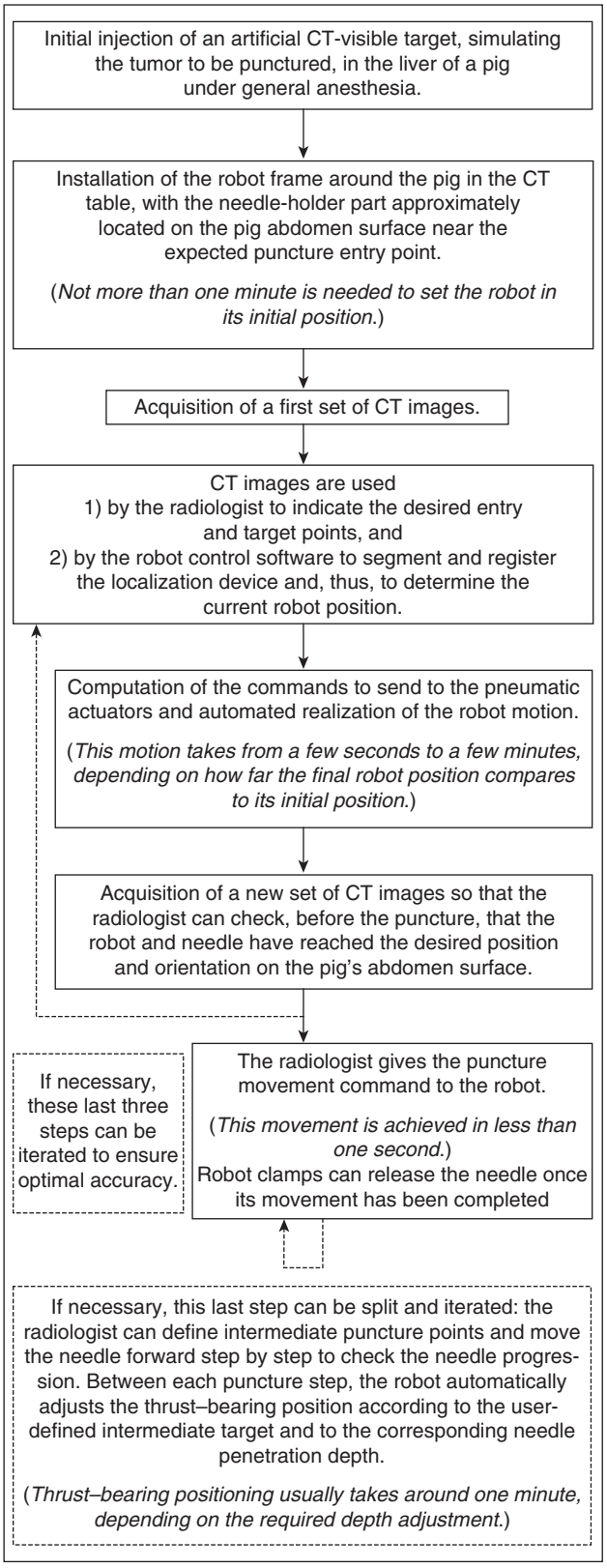

Fig. 9. Steps involved in the whole experimental setting.

Initial in vivo animal experiments on four pigs have been conducted within a CT environment [Figure 8(b)]. Figure 9 depicts steps involved in the whole experimental setting.

These preliminary in vivo experiments have demonstrated the feasibility of the LPR concept in clinical conditions. It should be noted that the robot had no difficulty in getting a rather large 17-gauge needle to penetrate pig skin, even though tissue stiffness is higher in pigs than that in humans. The resulting accuracies were measured within the range of 1 cm [Figure 8(c)]. This range can be considered as clinically acceptable, since any lesion measuring less than 1 cm in a patient is generally followed up by imaging. A more invasive decision such as biopsy or ablation is rarely taken unless the lesion gets larger than 1 cm.

Discussion and Conclusions

Translation accuracy of the robot over the patient's body surface has proved to be very satisfactory over small distances (less than 30 mm). Above this limit, the displacement is not as accurate; this is the counterpart of the body-supported strap-based translation design, where the robot is partially free to adjust its motion to the underlying surface. Nevertheless, since the loop is closed by CT-MR image acquisition and supervised by the physician, it is always possible to reach an excellent accuracy, as the physician can refine the robot position with an iterated translation. Ultimately, the final translation can always be set to be less than 30 mm. Under such conditions, experiments gave very promising results. The accuracy for orientation and inclination proved to be under 1°, and accuracy for the final puncture on a phantom with a depth up to 6 cm was less than 2 mm.

Preliminary in vivo experiments also gave results compatible with clinical applications, yet we can note that our in vivo experimental setting was particularly challenging [Figure 8(b) and (c)] for the following reasons:

1) Animal abdomens were significantly smaller than the usual human body. The robot had to translate over a nonflat surface with exaggerated curvature. Thus, the translation was less predictable. In this context, additional iterations can be useful to reach an optimized final puncture position.
2) The robot might also have been less stable in the small animal abdomen than in a flatter surface, even though the LPR weight, the strap tension, and the contact between the skin surface and the robot base allowed no visually detectable robot instability during positioning or puncture.
3) Last, but not least, it was not possible to obtain an apnea from the animals during our in vivo experiments. Thus, the larger part of the final puncture inaccuracy can be assumed to be due to respiratory motion.

These points require further in vivo evaluations. Segmentation and registration algorithms are currently based on image data acquired in a small volume that includes the localization device with postmotion processing. Further work will be done

to provide a fast closed-control loop, in real time during robot motion, based on a single-slice image acquisition.

Algorithms used during the LPR localization process have initially been developed with CT images. However, thanks to materials employed to construct the robot, to its compact architecture, and to the remote pneumatic energy source used to actuate it, LPR is fully MR-compatible, and image acquisitions with LPR have already been achieved in a clinical closed-bore MRI [Figure 1(a)].

An important point to consider when developing a medical device is the possibility of sterilizing the device components in contact with human body or protecting them with draping. The LPR is made of materials that are expected to be compatible with sterilization constraints; this point will deserve further experimental assessment.

Let us note that manipulating and driving a needle inside a closed MRI bore, and in the presence of a corpulent patient inside the bore, imposes a drastic limitation of the workspace [11]. Furthermore, this confined workspace is very dependent on the needle orientation and the patient size and position.

Indeed, during the experiments with the LPR, we have first measured the transversal workspace available between the patient's table and the inner MRI bore surface (a Philips Achieva, 60 cm Ø, 1.5 T) without any patient inside. At the midsagittal plane of the bore, this workspace is maximal and equals ~40 cm. When placing a male subject (1.65 m height and 65 kg weight) inside the MRI bore, the transversal workspace at the midsagittal plane of the bore is reduced to ~22 cm (the distance from the abdomen surface to the inner surface of the MRI bore). Off this midsagittal plane, due to the noncylindrical shape of patient's body, the workspace in an oblique plane can rapidly decrease to become as small as ~15 cm (see Figure 10).

However, if this workspace is able to contain the adequate needle chosen for the puncture, the intervention can also be performed using our needle driver under the condition that this latter presents a smaller (or equal) height than the chosen needle. The current prototype almost verifies this condition (15 cm height), and we are now working on the development of a smaller needle driver in which the height (~10 cm) will be compatible with the length of most existing biopsy needles. Presently, we are also adapting the CT segmentation and registration algorithms for MR images. This will allow the first LPR experiments with MRI on healthy volunteers and will further demonstrate the possibility with LPR to transform a simple CT or closed MR into a real-time controlled interventional imaging device.

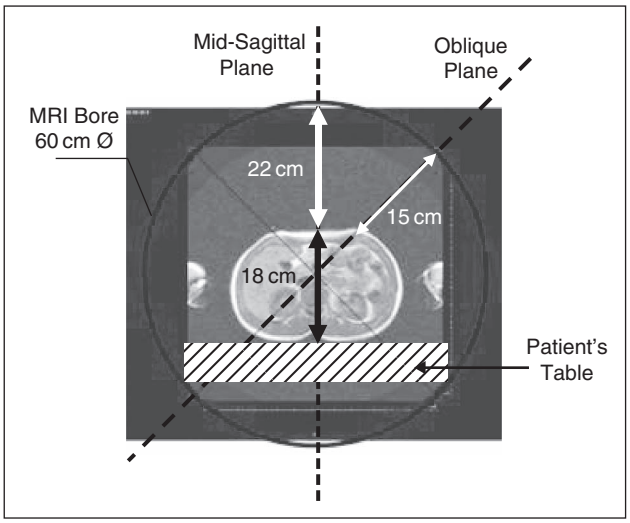

Fig. 10. A transversal MRI view of a patient's abdomen, emphasizing the limited workspace around the patient's abdomen inside a closed cylindrical MRI bore.

Acknowledgments

This work was partially funded by a grant from Ministère de la Recherche et de la Technologie, for Grenoble's Hospital Technology Innovation Center, and by a grant from Agence Nationale de la Recherche, for the Minimally Invasive Surgetics (SMI) project.

Ivan Bricault studied sciences and engineering at Ecole Polytechnique in Paris. He got a Ph.D. degree in applied mathematics in 1998 and an M.D. degree in 2002. He is a radiologist at the Grenoble University Hospital, specializing in abdominal imaging, and an assistant professor at the Grenoble Medical School. He works with the Computer-Assisted Medical Interventions research team at TIMC Laboratory.

Nabil Zemiti received his B.Sc. degree in electronics engineering from the University of Science of Algiers, Algeria, in 2001 and his M.Sc. degree in virtual reality and complex systems from the University of Versailles, France, in 2002. He obtained the Ph.D. degree in robotics from Paris 6 University, France, in 2005. From October 2002 to August 2006, he was a researcher at the Robotics Lab of Paris, University of Paris 6, France, where he was working on the force-feedback control of medical robots. He is currently a postdoctoral fellow at the TIMC-IMAG Laboratory, Grenoble, France, where he is working on computer-assisted medical interventions and sensor-based control for robotic manipulators.

Emilie Jouniaux received two M.S. degrees in 2006, one in information technologies for health from the Polytech Grenoble, France, and one in computer-assisted medicine and surgery from Grenoble's University of Medicine, France. She joined the Computer-Assisted Medical Interventions (CAMI) team of the TIMC Laboratory to work on the LPR and, especially, on its localization (image processing). Currently, she is a research and development engineer at Praxim Medivision, Grenoble, France.

Céline Fouard received her M.S. degree in computer science and image analysis from the University of Bordeaux, France, in 2001, and obtained her Ph.D. degree in computer science and medical image analysis at the University of Nice Sophia Antipolis, France, in 2005. In 2005–2006, she worked on image analysis at the Centre for Image Analysis, Uppsala University, Sweden, in the field of discrete geometry. Currently, she is an assistant professor at the TIMC-IMAG Lab, Université Joseph Fourier in Grenoble, France, where she teaches computer science and is working on computer-assisted medical interventions.

Élise Taillant received two M.S. degrees, one in telecommunications and signal processing from the National School of Applied Mathematics and Informatics (ENSIMAG) and another in computer-assisted medicine and surgery from Grenoble's University of Medicine. She started her professional career as a research and development engineer with the Gestes Médico-Chirurgicaux Assistés par Ordinateur (GMCAO) team of the TIMC Laboratory and, then, joined Praxim Medivision. In both the teams, she worked on the first prototype of the LPR, mainly on the robot control loop (CT and MR image processing, robot's localization algorithms, robot's control) and software development. She also led the first phantom tests in CT and MR environments. Currently, she is the research and development engineer of the Perception Team (ex-MOVI) at INRIA Rhône Alpes and works on a software for synchronized multiple-camera video playing and recording.

Frederic Dorandeu is the head of the Experimental Pharmacology and Toxicology Group within the Department of Toxicology, Centre de Recherches du Service de Santé des Armées (Military Medical Research Institute) in La Tronche, France. He received his pharmacy degree (Pharm. D.) from the University of Lyon, France, in 1990 and his Ph.D. degree in neurosciences from Université Joseph Fourier in 1998. He received two awards from the French National Academy of Pharmacy. He is a lieutenant-colonel in the French military health joint service. His group is primarily in charge of research on the medical countermeasures against the organophosphorus compound-induced toxicity.

Philippe Cinquin is a professor of medical informatics at TIMC-IMAG, a research unit of CNRS in Grenoble, France, and at Université Joseph Fourier. He heads the Centre for Technological Innovation of Grenoble's University Hospital. He holds a Ph.D. degree in applied mathematics and is a medical doctor. In 1984, he launched a research project on Computer Assisted Medical Interventions (CAMI). This activity lead to an innovative approach in surgical practice and to four industrial start-ups. He received the Maurice E. Muller award for excellence in computer-assisted orthopaedic surgery in 1999 and the CNRS silver medal in 2003.

Address for Correspondence: Ivan Bricault, Laboratoire TIMC, Equipe GMCAO, Institut d'Ingénierie de l'Information de Santé, Faculté de Médecine, 38706 La Tronche cedex, France. E-mail: ivan.bricault@imag.fr.

References

[1] R. H. Taylor and D. Stoianovici, "Medical robotics in computer-integrated surgery," *IEEE Trans. Robot. Automat.*, vol. 19, no. 5, pp. 765–781, Oct. 2003.

[2] K. Cleary, A. Melzer, V. Watson, G. Kronreif, and D. Stoianovici, "Interventional robotic systems: Applications and technology state-of-the-art," *Minim. Invasive Ther. Allied Technol.*, vol. 15, no. 2, pp. 101–113, Apr. 2006.

[3] J. F. Schenck, "The role of magnetic susceptibility in magnetic resonance imaging: MRI magnetic compatibility of the first and second kinds," *Med. Phys.*, vol. 23, no. 6, pp. 815–850, June 1996.

[4] K. Chinzei, R. Kikinis, and A. Jolesz, "MR compatibility of mechatronic devices: Design criteria," in *Proc. 2nd MICCAI*, Cambridge, Sept. 1999, pp. 1020–1031.

[5] K. Chinzei, K. Yoshinaka, and T. Washio, "Numerical simulations and lab tests for design of MR-compatible robots," in *Proc. IEEE Int. Conf. Robotics and Automation*, 2006, pp. 3819–3824.

[6] R. Gassert, R. Moser, E. Burdet, and H. Bleuler, "MRI/fMRI-compatible robotic system with force feedback for interaction with human motion," *IEEE/ASME Trans. Mechatron.*, vol. 11, no. 2, pp. 216–224, Apr. 2006.

[7] N. V. Tsekos, A. Özcan, and E. Christoforou, "A prototype manipulator for magnetic resonance-guided interventions inside standard cylindrical magnetic resonance imaging scanners," *J. Biomech. Eng.*, vol. 127, no. 6, pp. 972–980, Nov. 2005.

[8] B. T. Larson, N. V. Tsekos, A. G. Erdman, E. Yacoub, P. V. Tsekos, and I. G. Koutlas, "Design of an MR-compatible robotic stereotactic device for minimally invasive interventions in the breast," *J. Biomech. Eng.*, vol. 126, no. 4, pp. 458–465, Aug. 2004.

[9] H. Fischer, S. Kutter, J. Vagner, A. Felden, S. O. R. Pfleiderer, and W. A. Kaiser, "ROBITOM II: Robot for biopsy and therapy of the mamma," in *Proc. IEEE Int. Conf. Systems, Man and Cybernetics*, Oct. 2004, vol. 3. pp. 2530–2534.

[10] A. Krieger, R. C. Susil, C. Ménard, J. A. Coleman, G. Fichtinger, E. Atalar, and L. L. Whitcomb, "Design of a novel MR compatible manipulator for image guided prostate interventions," *IEEE Trans. Biomed. Eng.*, vol. 52, no. 2, pp. 306–313, Feb. 2005.

[11] K. Chinzei, N. Hata, A. Jolesz, and R. Kikinis, "Surgical assist robot for the active navigation in the intraoperative MRI: Hardware design issues," in *Proc. IEEE/RSJ Int. Conf. Intelligent Robots and Systems*, Takamatsu, Japan, 2000, vol. 1. pp. 727–732.

[12] Yamamoto, K. Ichiyanagi, T. Higuchi, H. Imamizu, R. Gassert, M. Ingold, L. Sache, and H. Bleuler, "Evaluation of MR-compatibility of electrostatic linear motor," in *Proc. IEEE Int. Conf. Robotics and Automation*, Barcelona, Spain, Apr. 2005, pp. 3658–3663.

[13] J. Vogan, A. Wingert, J. S. Plante, S. Dubowsky, M. Hafez, D. Kacher, and F. Jolesz, "Manipulation in MRI devices using electrostrictive polymer actuators: With an application to reconfigurable imaging coils," in *Proc. IEEE Int. Conf. Robotics and Automation*, May 2004, vol. 3. pp. 2498–2504.

[14] V. Gonzales, J. Troccaz, Ph. Cinquin, A. Guerraz, F. Pellisier, P. Thorel, B. Tondu, F. Courreges, G. Poisson, M. Althuser, and J.-M. Ayoubi, "Experiments with the TER tele-echography robot," in *Proc. 5th Int. Conf. Medical Image Computing and Computer-Assisted Intervention*, London, UK, 2002, vol. 2488. pp. 138–146.

[15] P. Berkelman, P. Cinquin, J. Troccaz, J. Ayoubi, C. Letoublon, and F. Bouchard, "A compact, compliant laparoscopic endoscope manipulator," in *Proc. IEEE Int. Conf. Robotics and Automation*, Washington, DC, May 2002, vol. 2. pp. 1870–1875.

[16] P. Cinquin, P. Berkelman, A. Jacquet, and J. Arnault, "System for positioning on a patient an observation and/or intervention device," International Patent BF 02/05848, May 13, 2002.

[17] N. Zemiti, G. Morel, T. Ortmaier, and N. Bonnet, "Mechatronic design of a new robot for force control in minimally invasive surgery," *IEEE/ASME Trans. Mechatron.*, vol. 12, no. 2, pp. 143–153, Apr. 2007.

[18] N. Zemiti, T. Ortmaier, M. Vitrani, and G. Morel, "A force controlled laparoscopic surgical robot without distal force sensing," in *Proc. 9th Int. Symp. Experimental Robotics*, Singapore, June 2004, pp. 153–163.

[19] J. Hong, T. Dohi, M. Hashizume, K. Konishi, and N. Hata, "An ultrasound-driven needle-insertion robot for percutaneous cholecystostomy," *Phys. Med. Biol.*, vol. 49, no. 3, pp. 441–455, 2004.

[20] B. Maurin, O. Piccin, B. Bayle, J. Gangloff, M. de Mathelin, L. Soler, and A. Gangi, "A new robotic system for CT-guided percutaneous procedures with haptic feedback," in *Proc. Computer Assisted Radiology and Surgery Congress*, Chicago, June 2004, pp. 515–520.

[21] R. C. Susil, J. H. Anderson, and R. H. Taylor, "A single image registration method for ct guided interventions," in *Proc. 2nd Int. Conf. Medical Image Computing and Computer-Assisted Intervention*, Cambridge, England, Sept. 1999, LNCS 1679, vol. 1679. pp. 798–808.

[22] G. Borgefors, "Hierarchical chamfer matching: A parametric edge matching algorithm," *IEEE Trans. Pattern Anal. Machine Intell.*, vol. 10, no. 6, pp. 849–865, Nov. 1988.

[23] Innomedic, Germany. (2008). INNOMOTION: CT- and MR-compatible assistance system for interventional radiology. [Online]. Available: www.innomedic.de

[24] R. Gassert, E. Burdet, and K. Chinzei, *IEEE Eng. Med. Biol. Mag.*, vol. 27, no. 3, pp. 15–22, 2008.